

# D2-Mamba: Dual-Scale Fusion and Dual-Path Scanning with SSMs for Shadow Removal

Linhao Li<sup>1</sup>, Boya Jin<sup>1</sup>, Zizhe Wang<sup>1</sup>, Lanqing Guo<sup>2\*</sup>, Hao Cheng<sup>1\*</sup>, Bo Li<sup>1</sup>, Yongfeng Dong<sup>1</sup>

<sup>1</sup> Hebei University of Technology, Tianjin, China

<sup>2</sup> The University of Texas at Austin, Austin, USA

{lilinhao, chenghao, dongyf}@hebut.edu.cn, {202332805034, 202422802032}@stu.hebut.edu.cn, {smurfsthen, deepblue.lb}@gmail.com

## Abstract

Shadow removal aims to restore images that are partially degraded by shadows, where the degradation is spatially localized and non-uniform. Unlike general restoration tasks that assume global degradation, shadow removal can leverage abundant information from non-shadow regions for guidance. However, the transformation required to correct shadowed areas often differs significantly from that of well-lit regions, making it challenging to apply uniform correction strategies. This necessitates the effective integration of non-local contextual cues and adaptive modeling of region-specific transformations. To this end, we propose a novel Mamba-based network featuring dual-scale fusion and dual-path scanning to selectively propagate contextual information based on transformation similarity across regions. Specifically, the proposed Dual-Scale Fusion Mamba Block (DFMB) enhances multi-scale feature representation by fusing original features with low-resolution features, effectively reducing boundary artifacts. The Dual-Path Mamba Group (DPMG) captures global features via horizontal scanning and incorporates a mask-aware adaptive scanning strategy, which improves structural continuity and fine-grained region modeling. Experimental results demonstrate that our method significantly outperforms existing state-of-the-art approaches on shadow removal benchmarks.

## Introduction

Shadows are common in natural images and often lead to visually distracting artifacts that adversely affect both human perception (Cucchiara et al. 2003; Nadimi and Bhanu 2004) and the performance of high-level vision tasks (Girshick et al. 2014; Yang et al. 2018; Özdemir and Akagündüz 2024). The goal of shadow removal is to restore clean, shadow-free images from inputs that are only partially degraded. Unlike other low-level restoration tasks, such as deblurring (Zou et al. 2021; Cho et al. 2021) or denoising (Pang et al. 2021; Zhu et al. 2025), which typically assume globally distributed degradation, shadow degradation is inherently spatially localized and non-uniform. This unique nature presents both opportunities and challenges: while non-shadow regions offer useful guidance for recovery, the corrections needed for shadow regions often differ greatly from those for well-lit regions, making uniform processing strategies ineffective.

\*Corresponding Author.

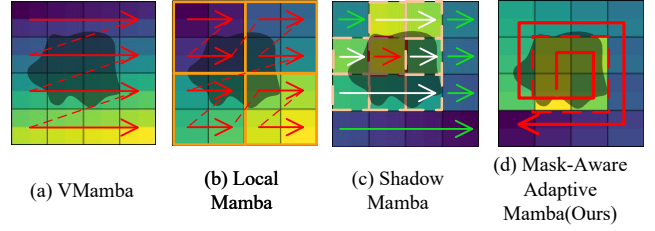


Figure 1: Illustrates four different Mamba scanning strategies on the SRD dataset: (a) VMamba (Liu et al. 2024b), sequential scanning with PSNR = 34.70; (b) LocalMamba (Huang et al. 2024), global scanning across windows with PSNR = 29.25; (c) ShadowMamba (Zhu, Chow, and Chuah 2024), a Mamba mechanism designed for shadow removal with PSNR = 33.63; (d) Ours, dynamically determines the scanning starting point based on the shadow mask and uses a breadth-first search algorithm to select the next patch to scan with PSNR = **35.13**.

Existing deep learning-based methods have made considerable progress by leveraging convolutional neural networks (CNNs) (Krizhevsky, Sutskever, and Hinton 2017) and, more recently, transformer architectures (Vaswani et al. 2017). CNN-based approaches (Chen et al. 2021; Li et al. 2023; Qu et al. 2017) often exploit local contextual cues but lack the capacity to capture long-range dependencies, which are crucial for understanding global scene structure and effectively transferring illumination and texture information across regions. Transformer-based models (Gillioz et al. 2020; He et al. 2021), in contrast, excel at capturing global interactions but often suffer from high computational cost, and their attention mechanisms may lack adaptability to the spatial heterogeneity introduced by shadows. More critically, both paradigms often apply a shared processing strategy across the entire image, overlooking the unique transformation requirements of shadowed versus non-shadowed regions. Recent attempts to address this limitation have explored multi-scale processing (Ding et al. 2018; Lu et al. 2023) or guided attention mechanisms (Fukui et al. 2019); however, these typically suffer from suboptimal fusion schemes or lack the ability to adaptively propagate context based on transformation similarity.

Recently, the State Space Model (SSM) architecture

Mamba has attracted widespread attention for simultaneously offering long-range modeling capability and linear computational complexity. As shown in Figure 1, for vision applications, researchers have explored various Mamba scanning strategies, including rigid row/column scans(Liu et al. 2024b), fixed local-window scans(Huang et al. 2024), and region-grouped scans(Zhu, Chow, and Chuah 2024). However, these methods struggle with issues like disrupting spatial adjacency or failing to capture global dependencies effectively. As a result, a more tailored framework that integrates transformation-aware adaptation and efficient context propagation remains highly desirable.

Based on this insight, we propose D2-Mamba, a novel Mamba-based network architecture specifically designed for shadow removal. Our design centers around two key innovations: (1) a Dual-Scale Fusion Mamba Block (DFMB) that fuses original and low-resolution features to enhance multi-scale representation and reduce boundary artifacts; and (2) a Dual-Path Mamba Group (DPMG) module that captures global structure using horizontal scanning while incorporating a mask-aware adaptive scanning strategy to preserve fine details and structural continuity across shadow and non-shadow regions. This strategy ensures that patches from the same region (shadow or non-shadow) are more closely grouped in the Mamba sequence, enhancing detail restoration. These two scanning mechanisms complement each other, improving the robustness of the entire module. As a result, the model can effectively capture shadow boundary information, reduce artifacts, and significantly enhance shadow removal quality. Extensive experiments on multiple benchmarks show that our method surpasses state-of-the-art models in PSNR, SSIM, and RMSE, while also delivering notable gains in efficiency and visual fidelity, validating its effectiveness for real-world shadow removal.

Our main contributions are summarized as follows:

- We propose a Dual-Path Mamba Group (DPMG), which integrates horizontal scanning and a mask-aware adaptive scanning strategy to enhance both global consistency and fine-grained detail recovery in shadow regions.
- We introduce a Dual-Scale Fusion Mamba Block (DFMB) that facilitates cross-layer information flow and feature fusion by leveraging scale-dependent representational differences in shadow regions, improving restoration quality in shadow areas.
- Extensive experiments on several datasets demonstrate that our method achieves state-of-the-art performance, while offering improved inference speed and computational efficiency.

## Related Work

**Shadow Removal.** Early deep learning-based shadow removal methods mainly relied on CNNs to map shadowed images to shadow-free counterparts. For example, Deshadownet (Qu et al. 2017) uses three jointly trained sub-networks to integrate semantic information for improved restoration. T-CGAN (Wang, Li, and Yang 2018) leverages stacked CGANs (Mirza and Osindero 2014) to generate both a mask and a shadow-free image, enhancing performance

through mutual task improvement. Mask-ShadowGAN (Hu et al. 2019) incorporates masks into the GAN (Goodfellow et al. 2020) framework, refining shadow region localization. Despite progress, CNN-based methods struggle with limited receptive fields, failing to capture long-range dependencies, particularly in complex illumination conditions. Transformer-based architectures (Vaswani et al. 2017) alleviates these issues by capturing long-range dependencies. HomoFormer (Xiao et al. 2024a) improves local self-attention adaptability by homogenizing shadow distributions, while ShadowFormer (Guo et al. 2023a) uses global attention to enhance boundary restoration. However, the high computational complexity of Transformers hinders their practical use in high-resolution tasks.

**State Space Models (SSMs).** SSMs have gained attention due to low computational complexity and strong ability to model long-range dependencies. The Structured State Space Sequence Model (S4) (Gu, Goel, and Ré 2021) introduced a linear-complexity hidden state update, boosting adoption in language and vision tasks (Sarem et al. 2024; Zhang et al. 2025; Nasiri-Sarvi et al. 2024). Mamba further improved this with parallel computation and a refined update scheme.

SSMs have recently been applied to low-level vision tasks such as image super-resolution (Lei, Zhang, and Cao 2024; Qiao et al. 2024; Xiao et al. 2024b) and denoising (Lu et al. 2024; Zhu et al. 2025), showing significant improvements in computational efficiency and reconstruction quality. MambaIR (Vasluianu et al. 2024) introduced a selective SSM approach for image restoration, enhancing reconstruction quality. LocalMamba (Huang et al. 2024) utilized a local window scanning strategy to improve local interactions while retaining global context. Hi-mamba (Qiao et al. 2024) proposed a hierarchical Mamba structure for better multi-scale information fusion and feature representation.

For shadow removal, general Mamba models often fail to account for the unique characteristics of shadow images, disrupting semantic relationships at boundaries. Shadow-Mamba (Zhu, Chow, and Chuah 2024) introduced a selective scanning strategy for region-based partitioning, but its rigid partitioning limits adaptability. To address these issues, we enhance cross-layer information fusion and introduce a mask-aware scanning mechanism for better structural continuity and region modeling.

## Method

### Preliminaries

State Space Model (SSM) is a mathematical framework used to describe and analyze dynamic systems. It characterizes the internal state of a system through state variables and establishes the relationships between the state, input, and output. Specifically, an SSM maps a one-dimensional input sequence  $x(t) \in \mathbb{R}$  to an output sequence  $y(t) \in \mathbb{R}$  while propagating information through a hidden state  $h(t) \in \mathbb{R}^N$ . Its continuous-time formulation can be expressed by the following differential equations.

$$\begin{cases} h'(t) = Ah(t) + Bx(t) \\ y(t) = Ch(t) + Dx(t) \end{cases} \quad (1)$$

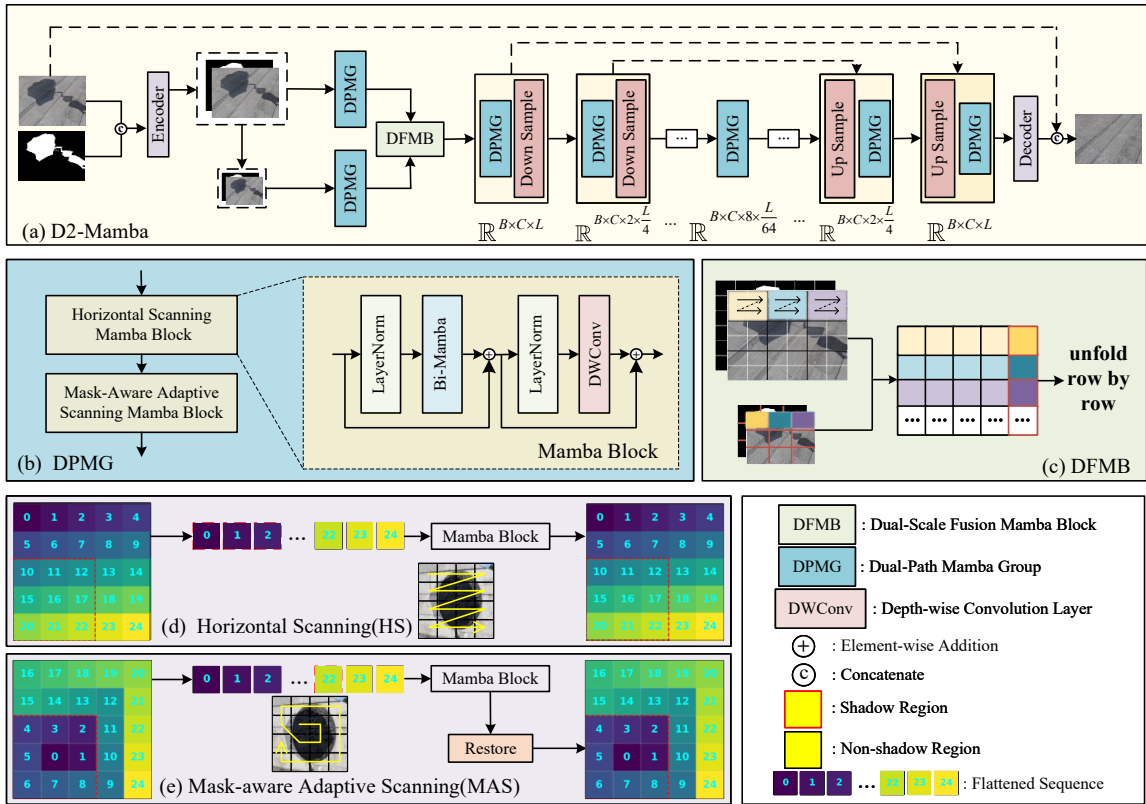


Figure 2: (a) An overview of our proposed D2-Mamba framework consisting of two core modules: (b) Dual-Path Mamba Group (DPMG) extracts global context information through one path using the (d) Horizontal Scanning strategy and (e) Mask-aware Adaptive scanning strategy; (c) Dual-Scale Fusion Mamba Block (DFMB) enhances the model’s ability to capture multi-scale contextual information by fusing original resolution and downsampled features.

where  $A \in \mathbb{R}^{N \times N}$  governs the state transition, while  $B \in \mathbb{R}^{N \times 1}$  and  $C \in \mathbb{R}^{1 \times N}$  establish the relationships between the input and state, as well as the state and output, respectively. The term  $D$  represents the direct transmission component.

To enable discrete sequence processing in deep learning, the continuous  $A$  and  $B$  are discretized into  $\bar{A}$  and  $\bar{B}$ :

$$\begin{cases} \bar{A} = \exp(\Delta A) \\ \bar{B} = (\Delta A)^{-1}(\exp(\Delta A) - I) \cdot \Delta B \end{cases} \quad (2)$$

Furthermore, SSM can be efficiently computed in a convolutional form. By expanding the discretized parameters into a structured convolutional kernel  $\bar{K} \in \mathbb{R}^L$  (where  $L$  represents the sequence length), the output can be expressed as the convolution of the input sequence  $x$  with  $\bar{K}$ , where “ $*$ ” denotes the convolution operation:

$$y = x * \bar{K}, \quad \bar{K} = (C\bar{B}, C\bar{A}\bar{B}, \dots, C\bar{A}^{L-1}\bar{B}). \quad (3)$$

In traditional SSM, the parameters  $A$ ,  $B$ ,  $C$ , and  $\Delta$  are fixed values, while Mamba builds on S4 by making them input-dependent, achieving both linear complexity and greater modeling flexibility.

## Overall Architecture

Figure 2 presents an overview of the proposed D2-Mamba framework, which includes a feature encoder, a DFMB mod-

ule, a UNet built with DPMG blocks, and a feature decoder.

The encoder takes the concatenated shadow image and mask as input, producing compact features  $F_t \in \mathbb{R}^{L \times C}$ , where  $L$  denotes the spatial dimension (*i.e.*, the product of image height and width) and  $C$  the number of channels. These features are processed at two different scales by DFMB, which fuses them to enhance global semantics and capture shadow distributions effectively. The fused features are subsequently processed by a UNet-like architecture composed of DPMG modules. DPMG integrates two global scanning strategies: a horizontal Z-shaped scan and a mask-aware adaptive scan that prioritizes shadow regions. These strategies help the model better capture shadow structures and boundaries. The UNet-like architecture performs four downsampling and four upsampling operations with a central bottleneck, gradually compressing and restoring the spatial resolution. Finally, the decoder generates the shadow-free output. By combining dual-scale feature fusion with complementary scanning paths, D2-Mamba enables efficient and robust removal of complex shadows.

## Dual-Path Mamba Group

To effectively handle the distinct transformation requirements of shadow and non-shadow regions, we propose a dual-path Mamba group module incorporating a dual scan-

ning strategy (Figure 2(b)). Specifically, a mask-aware adaptive scanning mechanism is employed to group and process shadow regions, ensuring consistent transformations within shadow areas. In parallel, a horizontal scanning pathway captures local continuity and contextual information across both shadow and non-shadow regions, thereby enhancing the overall information flow and integration.

As shown in Figure 2(d), the HSMB employs a row-wise scanning strategy. Given an input feature map  $X \in \mathbb{R}^{C \times H \times W}$ , we flatten it into a sequence  $V \in \mathbb{R}^{C \times (H \times W)}$  and apply bidirectional scanning (left-to-right and right-to-left), enabling feature interactions in a single step. Each Mamba block uses ConvMLP with two fully connected layers for feature transformation. The first layer projects features into a high-dimensional space, followed by depthwise separable convolution (DWConv) for local feature enhancement. After passing through GELU and Dropout, the features are projected back to the original dimension:

$$z = \text{Dropout}(W_2(\text{GELU}(\text{DWConv}(W_1x))))). \quad (4)$$

HSMB captures long-range dependencies via a bidirectional state update, effectively modeling regional correlations and enhancing feature representation.

**Mask-aware Adaptive Scanning.** After establishing long-range dependencies with HSMB, we propose a novel Mask-aware Adaptive Scanning (MAS) to improve structural continuity and fine-grained region modeling. In the shadow regions, we employ a spiral scan, while for the non-shadow areas, we adopt the Greedy Boundary-contact Search (GBS) strategy to ensure scan continuity. The detailed search process of the proposed mask-aware adaptive scanning strategy is outlined in Algorithm 1.

For clarity, we use the example shown in Figure 2(e). In this case, we first perform spatial partitioning based on the input feature map  $x \in \mathbb{R}^{C \times H \times W}$  and the shadow mask  $m \in \mathbb{R}^{1 \times H \times W}$ , dividing the image into  $\frac{H}{8} \times \frac{W}{8}$  sub-blocks of size  $s \times s$ . The average mask value  $\bar{m}_{i,j}$  of each sub-block is then computed to determine whether it belongs to the shadow region. At this point, the image has  $r$  rows and  $c$  columns, and the shadow region has  $\text{sub}_r$  rows and  $\text{sub}_c$  columns. We then compute the center position of the shadow block as  $(cx_{\text{sub}}, cy_{\text{sub}})$  and calculate the distance to the image boundaries as follows:

$$\begin{cases} t = \max(0, cx_{\text{sub}} - \frac{\text{sub}_r-1}{2}) \\ b = \min(r-1, cx_{\text{sub}} + \lfloor \frac{\text{sub}_r}{2} \rfloor) \\ l = \max(0, cy_{\text{sub}} - \frac{\text{sub}_c-1}{2}) \\ r = \min(c-1, cy_{\text{sub}} + \lfloor \frac{\text{sub}_c}{2} \rfloor) \end{cases} \quad (5)$$

Using these distances, we set the starting point for the non-shadow region as  $\text{start}_A$ . Next, the GBS strategy is employed to find the next grid with the most boundary contacts to the previously visited grid, which is then added to the path  $\text{path}_A$ . For the shadow region, we select the closest point to the starting point of the non-shadow area as the initial point  $\text{start}_B$  and apply a spiral path inward, reversing it to obtain  $\text{path}_B$ . The final sequence is  $\text{path} = [\text{path}_B, \text{path}_A]$ , and we apply the Mamba and ConMLP models to perform feature transformation and modeling.

---

#### Algorithm 1: Mask-Aware Adaptive Scanning Strategy

---

**Input:**  $r; c; \text{sub}_r; \text{sub}_c; cx_{\text{sub}}; cy_{\text{sub}}; \text{directions} = \{(-1,0), (1,0), (0,-1), (0,1)\}$ .

**Output:**  $\text{path}$

```

1: Select the Starting Point of Non-Shadow Region A:
2:  $t, b, l, r \leftarrow \text{rect\_bounds}(r, c, \text{sub}_r, \text{sub}_c, cx_{\text{sub}}, cy_{\text{sub}})$ 
3:  $\text{dist} \leftarrow \{t, b, l, r\}$  #Distance to each edge of full image
4:  $\text{edge1} \leftarrow \text{choose\_closest\_edge}(\text{dist})$ 
5:  $\text{edge2} \leftarrow \text{choose\_adjacent\_edge}(\text{dist}, \text{edge1})$ 
6:  $\text{start}_A \leftarrow (\text{edge1}, \text{edge2})$ 
7: Traverse Non-Shadow Region A:
8:  $\text{visited} \leftarrow \{(x, y) \mid t \leq x \leq b, l \leq y \leq r\}$ 
9:  $\text{path}_A \leftarrow []$ 
10: while  $|\text{visited}| < r \times c$  do
11:    $\text{best} \leftarrow \text{None}, \text{best\_touch} \leftarrow -1, \text{eq} = []$ 
12:   for each  $(dr, dc) \in \text{directions}$  do
13:      $nr, nc \leftarrow \text{cur}[0] + dr, \text{cur}[1] + dc$ 
14:      $\text{touch} = \text{calculate\_touch}(nr, nc)$ 
15:     if  $\text{touch} > \text{best\_touch}$  then
16:        $\text{candList} \leftarrow (nr, nc), \text{best\_touch} \leftarrow \text{touch}$ 
17:     else if  $\text{touch} == \text{best\_touch}$  then
18:        $\text{candList} \leftarrow \text{candList} \cup \{(nr, nc)\}$ 
19:     end if
20:   end for
21:   if  $\text{candList}$  is None then
22:      $\text{best} \leftarrow \text{min\_manhattan}(\text{unvisited})$ 
23:   else
24:      $\text{best} \leftarrow \text{select\_candlist}(\text{candList})$ 
25:   end if
26:    $\text{cur} \leftarrow \text{best}$ 
27:    $\text{visited} \leftarrow \text{visited} \cup \{\text{cur}\}$ 
28:   if  $(\text{cur}[0], \text{cur}[1]) \notin B$  then
29:      $\text{path}_A \leftarrow \text{path}_A \cup \{\text{cur}\}$ 
30:   end if
31: end while
32: Traverse Shadow Region B:
33:  $\text{start}_B \leftarrow \text{choose\_closest\_point\_in\_B}(\text{start}_A)$ 
34:  $\text{path}_B \leftarrow \text{reversr}(\text{spiral\_in}(\text{start}_B))$ 
35: return  $\text{path}_B \cup \text{path}_A$ 

```

---

#### Dual-Scale Fusion Mamba Block

Previous studies (Ren et al. 2024; Guo et al. 2023a) demonstrate that cross-scale information is crucial for achieving consistent brightness and color in shadow removal. To further incorporate cross-scale information into the Mamba framework, we draw inspiration from the position-aligned cross-scale scanning strategy proposed by MambaCSR (Ren et al. 2024). Building on this idea, we design an improved cross-scale feature fusion strategy to leverage multi-scale features and enhance the restoration capability effectively.

First, the input shadow image  $I_s$  and its binary shadow mask  $M$  are fed into the encoder to extract the initial feature:

$$F_{\text{input}} = \text{Flatten}(\text{LeakyReLU}(\text{Conv2d}(\text{Concat}(I_s, M))))). \quad (6)$$

To incorporate richer information, we apply bilinear interpolation to downsample the original feature map, obtaining a lower-resolution representation  $F_{\text{down}}$ . Both  $F_{\text{input}}$  and  $F_{\text{down}}$

Method	Shadow Region (S)			Non-Shadow Region (NS)			All Image (ALL)		
	PSNR $\uparrow$	SSIM $\uparrow$	RMSE $\downarrow$	PSNR $\uparrow$	SSIM $\uparrow$	RMSE $\downarrow$	PSNR $\uparrow$	SSIM $\uparrow$	RMSE $\downarrow$
DeshadowNet (Qu et al. 2017)	-	-	11.78	-	-	4.84	-	-	6.64
DHAN (Chen et al. 2021)	33.67	0.978	8.94	34.79	0.979	4.80	30.51	0.949	5.67
BMNet (Zhu et al. 2022)	35.05	0.981	6.61	36.02	0.982	3.61	31.69	0.956	4.46
SGNet (Wan et al. 2022)	33.76	0.979	7.45	36.48	0.984	3.05	31.39	0.960	4.23
ShadowFormer-L (Guo et al. 2023a)	36.91	<b>0.989</b>	5.90	36.22	<b>0.989</b>	3.44	32.90	0.958	4.04
ShadowDiffusion (Guo et al. 2023b)	<u>38.72</u>	<u>0.987</u>	4.98	37.78	0.985	3.44	34.73	<u>0.970</u>	3.63
HomoFormer (Xiao et al. 2024a)	<b>38.81</b>	<u>0.987</u>	<b>4.25</b>	<u>39.45</u>	<u>0.988</u>	<u>2.85</u>	<u>35.37</u>	<b>0.972</b>	<u>3.33</u>
Liu et al. (Liu et al. 2024a)	36.51	0.983	5.49	37.71	0.986	3.00	33.48	0.967	3.66
ShadowMamba (Zhu, Chow, and Chuah 2024)	37.29	0.986	5.81	37.52	0.985	3.13	33.63	0.965	3.87
ShadowGAN-Former (Hu et al. 2025)	35.24	0.981	6.578	36.12	0.981	3.54	31.73	0.956	4.39
ShadowMaskFormer (Li et al. 2025)	37.71	0.988	5.55	38.23	0.984	2.98	34.43	0.968	3.64
MSRDNet (Huang et al. 2025)	35.43	0.984	5.98	36.23	0.989	3.38	32.17	0.965	4.09
OmniSR (Xu et al. 2025)	-	-	-	-	-	-	34.56	0.977	-
D2-Mamba (Ours)	38.46	0.981	<u>4.38</u>	<b>40.02</b>	0.983	<b>2.77</b>	<b>35.41</b>	0.958	<b>3.31</b>

Table 1: The quantitative results of shadow removal on SRD dataset. The best and the second results are in bold and underlined.

Method	Shadow Region (S)			Non-Shadow Region (NS)			All Image (ALL)		
	PSNR $\uparrow$	SSIM $\uparrow$	RMSE $\downarrow$	PSNR $\uparrow$	SSIM $\uparrow$	RMSE $\downarrow$	PSNR $\uparrow$	SSIM $\uparrow$	RMSE $\downarrow$
DHAN (Chen et al. 2021)	32.92	0.988	9.6	27.15	0.971	7.4	25.66	0.956	7.8
SGNet (Wan et al. 2022)	36.79	0.990	5.9	35.57	<u>0.977</u>	2.9	32.45	0.962	3.4
BMNet (Zhu et al. 2022)	37.87	<u>0.991</u>	5.8	37.51	<b>0.985</b>	2.4	33.98	0.972	3.0
ShadowFormer-L (Guo et al. 2023a)	39.67	-	5.2	38.82	-	2.3	35.46	-	2.8
ShadowDiffusion (Guo et al. 2023b)	<u>39.8</u>	-	<u>4.9</u>	<u>38.90</u>	-	<u>2.3</u>	<u>35.72</u>	-	<u>2.7</u>
HomoFormer (Xiao et al. 2024a)	39.49	<u>0.991</u>	<u>4.9</u>	38.64	0.982	2.3	35.31	0.969	<b>2.6</b>
Liu et al. (Liu et al. 2024a)	38.04	0.990	5.7	39.15	<u>0.984</u>	2.3	34.96	0.968	2.9
ShadowMamba (Zhu, Chow, and Chuah 2024)	-	-	5.8	-	-	<u>2.3</u>	-	-	2.8
MSRDNet (Huang et al. 2025)	38.93	<u>0.991</u>	5.5	38.49	<b>0.985</b>	2.4	34.94	<u>0.972</u>	2.9
OmniSR (Xu et al. 2025)	-	-	-	-	-	-	34.20	<b>0.973</b>	-
D2-Mamba (Ours)	<b>40.22</b>	<b>0.992</b>	<b>4.6</b>	<b>38.95</b>	<b>0.985</b>	<b>2.2</b>	<b>35.84</b>	<b>0.973</b>	<b>2.6</b>

Table 2: The quantitative results of shadow removal on the ISTD+ dataset.

are subsequently processed by DPMG to model global and region-level dependencies from different shadow areas.

For feature fusion, we adopt a position-aligned unfolding strategy. As shown in Figure 2(c), for any pixel  $x_d(i, j)$  in the downsampled feature map  $F_{\text{down}}$ , we extract its four spatially aligned neighbors from the original feature map  $F_{\text{input}}: x(2i, 2j), x(2i+1, 2j), x(2i, 2j+1), x(2i+1, 2j+1)$ , which are then grouped into a sequential token unit:

$$S_{i,j} = [x(2i, 2j), x(2i+1, 2j), x(2i, 2j+1), x(2i+1, 2j+1), x_d(i, j)], i \in [1, H/2], j \in [1, W/2]. \quad (7)$$

Next, we perform a row-wise scan of the fused feature map  $S_{i,j}$ , unfolding each five-element group in a sequential order to generate a 1D sequence  $S$ . This sequence is fed into the fusion mamba block to obtain  $F_{\text{fused}}$  for fine-grained multi-scale feature interaction.

The fused features  $F_{\text{fused}}$  are then forwarded to the subsequent U-Net structure for further processing. During the downsampling stage, the U-Net stores the intermediate features generated by the Mamba module, *i.e.*,  $x_s \in$

$\mathbb{R}^{C \times H/s \times W/s}$ , which are later upsampled and aligned back to the original spatial resolution  $x' \in \mathbb{R}^{C \times H \times W}$ . These features are fused with corresponding encoder features in the upsampling path, allowing the network to better preserve structure and detail for more refined shadow removal.

## Experiments

### Experimental Setups

**Datasets.** We conduct experiments on three widely used shadow removal benchmarks: SRD (Qu et al. 2017), ISTD (Wang, Li, and Yang 2018), and ISTD+ (Le and Samarasinghe 2019). The SRD dataset contains 3,088 shadow/shadow-free image pairs. Since it lacks ground-truth shadow masks, we use predicted masks from DHAN (Chen et al. 2021) as substitutes. We follow the standard split with 2,680 pairs for training and 408 for testing. The ISTD dataset provides 1,870 triplets, each consisting of a shadow image, its mask, and a corresponding shadow-free image, divided into 1,330 training and 540 testing samples. ISTD+ is an improved



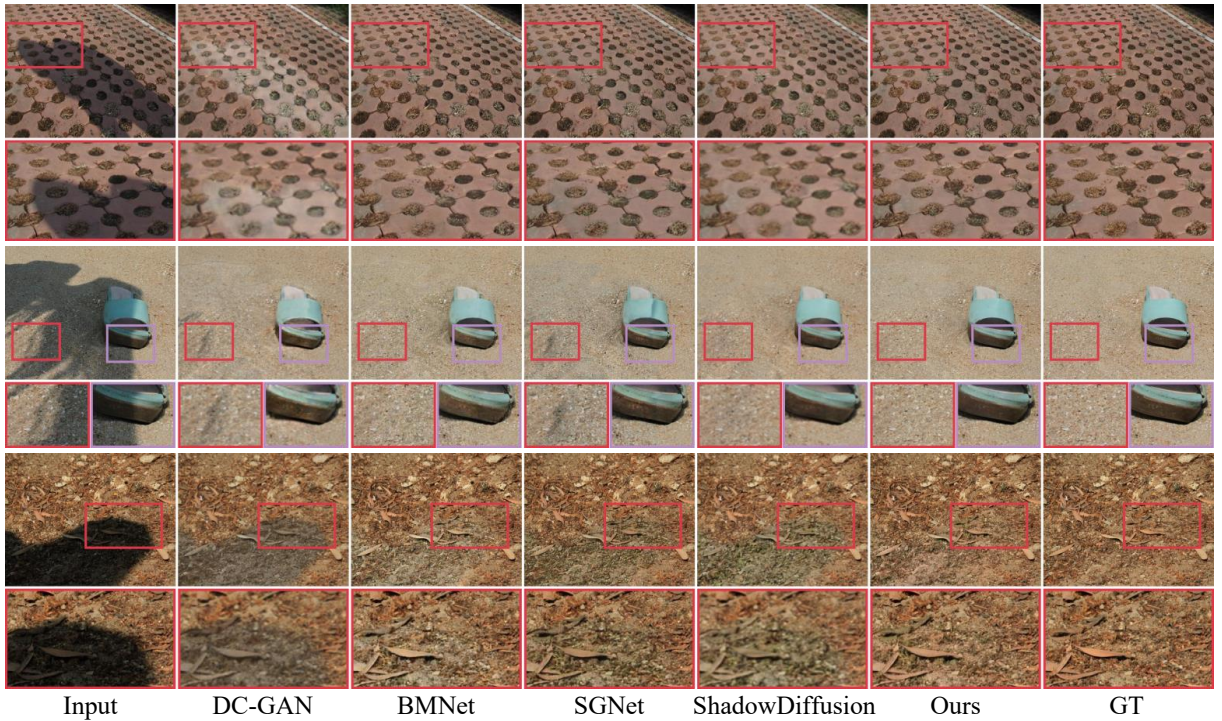


Figure 3: Visual comparisons with state-of-the-art methods on the SRD dataset.

version of ISTD, in which illumination inconsistencies between shadow and shadow-free images have been corrected through post-processing techniques.

**Implementation Details.** Our method is optimized using the Adam optimizer (Kingma and Ba 2014) and implemented in the PyTorch framework. All experiments were conducted on a single NVIDIA RTX 4090 GPU. The initial learning rate for training is set to  $2 \times 10^{-4}$ , with momentum parameters  $\beta_1$  and  $\beta_2$  set to 0.9 and 0.999, respectively, and a batch size of 4. To optimize the training process, a cosine annealing strategy is employed to gradually reduce the learning rate, ultimately converging to  $1 \times 10^{-6}$ .

### Comparison with State-of-the-Art

We compare the proposed model with popular or state-of-the-art shadow removal methods. Results of all comparison methods are either obtained from their original publications or reproduced using official implementations<sup>1</sup>.

**Quantitative evaluation.** Table 1 and Table 2 present the quantitative evaluation results over SRD and ISTD+, respectively. Our method consistently outperforms or matches existing approaches across multiple evaluation metrics, demonstrating its effectiveness and robustness in shadow removal. On the SRD dataset, which contains more complex scenes and textures, diffusion-based methods perform well due to their strong generative capacity for modeling intricate details, significantly outperforming traditional regression-based approaches. However, their long inference

time and limited scalability to high-resolution inputs remain key drawbacks. In contrast, our Mamba-based regression model, equipped with accurate cross-scale fusion and similarity-aware grouping, achieves competitive or superior performance with far fewer inference steps, making it both efficient and practical for real-world deployment.

**Qualitative evaluation.** To further validate visual effectiveness, we provide qualitative comparisons on SRD and ISTD+, which cover diverse scenes with varying shadow shapes, densities, and lighting conditions, providing a comprehensive evaluation of robustness. Figures 3 and 4 clearly show that our method consistently achieves smoother shadow boundaries and more complete removal of residual artifacts compared to other approaches. Some methods produce shadow-recovered regions that appear noticeably brighter or darker than their surroundings (e.g., first and third examples in Figure 3), while others struggle with boundary artifacts (e.g., second and fourth examples). These limitations become more evident in challenging scenarios, such as high-saturation scenes in Figure 4, which often lead to color inconsistencies. In contrast, our approach effectively removes shadow artifacts while restoring natural luminance and color, resulting in improved global consistency and visual realism.

### Ablation Study

We conduct ablation studies on SRD to assess the effectiveness of D2-Mamba’s key components. Table 3 shows that each component contributes to performance gains.

**Effects of DFMB.** In the encoding stage, we introduced

<sup>1</sup>Evaluation metrics for all datasets and experimental results on the ISTD dataset are provided in Appendix.

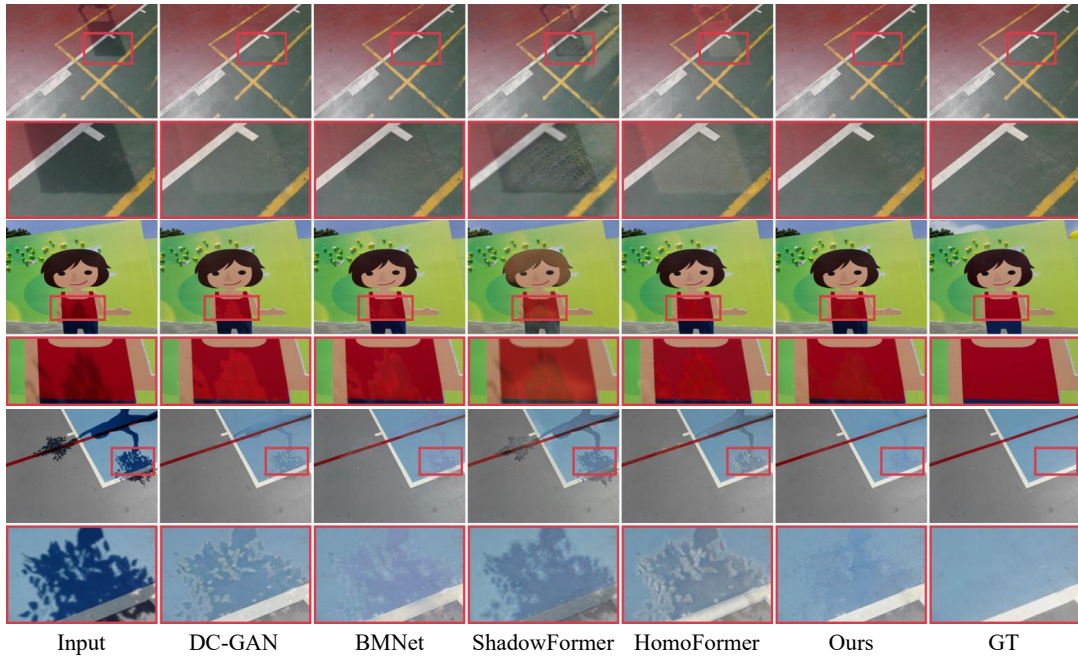


Figure 4: Visual comparisons with state-of-the-art methods on the ISTD+ dataset.

	DFMB	DPMG		Shadow Region (S)			Non-Shadow Region (NS)			All Image (ALL)		
		HS	MAS	PSNR $\uparrow$	SSIM $\uparrow$	RMSE $\downarrow$	PSNR $\uparrow$	SSIM $\uparrow$	RMSE $\downarrow$	PSNR $\uparrow$	SSIM $\uparrow$	RMSE $\downarrow$
1	—	✓	—	37.92	0.980	4.60	39.58	0.981	2.85	34.87	0.955	3.44
2	—	—	✓	37.54	0.978	4.72	39.09	0.979	2.94	34.47	0.950	3.53
3	—	✓	✓	38.17	0.981	4.48	39.82	0.982	2.82	35.13	0.956	3.37
4	✓	✓	✓	38.52	0.981	4.37	40.03	0.982	2.76	35.42	0.958	3.30

Table 3: Ablation study of the proposed D2-Mamba on the SRD dataset.

DFMB, which establishes dual-scale aggregation paths to effectively integrate features at different spatial resolutions. By fusing contextual information from both coarse and fine scales, DFMB enhances the capacity to capture global semantics and local details. This not only enriches the feature representation but also stabilizes the input to the UNet, resulting in more discriminative and consistent features. Ablation results show that removing DFMB causes a significant drop in PSNR and a noticeable increase in RMSE, especially in complex regions with fine shadow details.

**Effects of DPMG.** To handle the distinct characteristics of shadow and non-shadow regions, we propose the DPMG, which integrates HS and MAS. Using HS alone promotes global structural consistency but applies uniform processing across the entire image, neglecting the specific needs of shadow regions. Conversely, MAS enhances illumination and color fidelity within shadow areas but lacks sufficient global context, often resulting in texture degradation or boundary blurring. The combined DPMG module leverages the strengths of both: HS preserves structural coherence, while MAS adaptively refines shadow recovery. This design leads to significant gains in PSNR and improved boundary

continuity, while effectively reducing visual artifacts.

## Conclusion

This paper proposes a novel shadow removal method based on dual-scale fusion and dual-path mask-aware Mamba. The designed DFMB module enhances the model’s ability to extract contextual information effectively through a dual-scale fusion mechanism, stabilizing the diversity of input features. The DPMG module combines the advantages of global horizontal scanning and shadow-priority scanning, effectively leveraging global information while ensuring local consistency, thereby significantly improving the recovery of shadow regions. Extensive experimental evaluations on SRD, ISTD, and ISTD+, demonstrate that our method achieves leading performance across various evaluation metrics, particularly excelling in detail preservation and restoration of image brightness and color consistency. These results indicate that our method provides an efficient and robust solution for the shadow removal task. Future research could further explore the potential in more complex scenarios and shadow patterns, thereby improving the generalizability.

## References

- Chen, Z.; Long, C.; Zhang, L.; and Xiao, C. 2021. Canet: A context-aware network for shadow removal. In *Proceedings of the IEEE/CVF international conference on computer vision*, 4743–4752.
- Cho, S.-J.; Ji, S.-W.; Hong, J.-P.; Jung, S.-W.; and Ko, S.-J. 2021. Rethinking coarse-to-fine approach in single image deblurring. In *Proceedings of the IEEE/CVF international conference on computer vision*, 4641–4650.
- Cucchiara, R.; Grana, C.; Piccardi, M.; and Prati, A. 2003. Detecting moving objects, ghosts, and shadows in video streams. *IEEE transactions on pattern analysis and machine intelligence*, 25(10): 1337–1342.
- Ding, H.; Jiang, X.; Shuai, B.; Liu, A. Q.; and Wang, G. 2018. Context contrasted feature and gated multi-scale aggregation for scene segmentation. In *Proceedings of the IEEE conference on computer vision and pattern recognition*, 2393–2402.
- Fu, L.; Zhou, C.; Guo, Q.; Juefei-Xu, F.; Yu, H.; Feng, W.; Liu, Y.; and Wang, S. 2021. Auto-exposure fusion for single-image shadow removal. In *Proceedings of the IEEE/CVF conference on computer vision and pattern recognition*, 10571–10580.
- Fukui, H.; Hirakawa, T.; Yamashita, T.; and Fujiyoshi, H. 2019. Attention branch network: Learning of attention mechanism for visual explanation. In *Proceedings of the IEEE/CVF conference on computer vision and pattern recognition*, 10705–10714.
- Gillioz, A.; Casas, J.; Mugellini, E.; and Abou Khaled, O. 2020. Overview of the Transformer-based Models for NLP Tasks. In *2020 15th Conference on computer science and information systems (FedCSIS)*, 179–183. IEEE.
- Girshick, R.; Donahue, J.; Darrell, T.; and Malik, J. 2014. Rich feature hierarchies for accurate object detection and semantic segmentation. In *Proceedings of the IEEE conference on computer vision and pattern recognition*, 580–587.
- Goodfellow, I.; Pouget-Abadie, J.; Mirza, M.; Xu, B.; Warde-Farley, D.; Ozair, S.; Courville, A.; and Bengio, Y. 2020. Generative adversarial networks. *Communications of the ACM*, 63(11): 139–144.
- Gu, A.; Goel, K.; and Ré, C. 2021. Efficiently modeling long sequences with structured state spaces. *arXiv preprint arXiv:2111.00396*.
- Guo, L.; Huang, S.; Liu, D.; Cheng, H.; and Wen, B. 2023a. Shadowformer: global context helps shadow removal. In *Proceedings of the AAAI conference on artificial intelligence*, volume 37, 710–718.
- Guo, L.; Wang, C.; Yang, W.; Huang, S.; Wang, Y.; Pfister, H.; and Wen, B. 2023b. Shadowdiffusion: When degradation prior meets diffusion model for shadow removal. In *Proceedings of the IEEE/CVF Conference on Computer Vision and Pattern Recognition*, 14049–14058.
- He, S.; Luo, H.; Wang, P.; Wang, F.; Li, H.; and Jiang, W. 2021. Transreid: Transformer-based object re-identification. In *Proceedings of the IEEE/CVF international conference on computer vision*, 15013–15022.
- Hu, J.; Wen, S.; Li, J.; and Karimi, H. R. 2025. ShadowGAN-Former: Reweighting self-attention based on mask for shadow removal. *Neural Networks*, 107175.
- Hu, X.; Jiang, Y.; Fu, C.-W.; and Heng, P.-A. 2019. Mask-shadowgan: Learning to remove shadows from unpaired data. In *Proceedings of the IEEE/CVF international conference on computer vision*, 2472–2481.
- Huang, T.; Pei, X.; You, S.; Wang, F.; Qian, C.; and Xu, C. 2024. Localmamba: Visual state space model with windowed selective scan. *arXiv preprint arXiv:2403.09338*.
- Huang, Y.; Lu, X.; Quan, Y.; Xu, Y.; and Ji, H. 2025. Image shadow removal via multi-scale deep Retinex decomposition. *Pattern Recognition*, 159: 111126.
- Kingma, D. P.; and Ba, J. 2014. Adam: A method for stochastic optimization. *arXiv preprint arXiv:1412.6980*.
- Krizhevsky, A.; Sutskever, I.; and Hinton, G. 2017. ImageNet classification with deep convolutional neural networks. *Communications of the ACM*, 84–90.
- Le, H.; and Samarasinghe, D. 2019. Shadow removal via shadow image decomposition. In *Proceedings of the IEEE/CVF International Conference on Computer Vision*, 8578–8587.
- Le, H.; and Samarasinghe, D. 2021. Physics-based shadow image decomposition for shadow removal. *IEEE Transactions on Pattern Analysis and Machine Intelligence*, 44(12): 9088–9101.
- Lei, X.; Zhang, W.; and Cao, W. 2024. Dvmsr: Distillated vision mamba for efficient super-resolution. In *Proceedings of the IEEE/CVF Conference on Computer Vision and Pattern Recognition*, 6536–6546.
- Li, X.; Guo, Q.; Abdelfattah, R.; Lin, D.; Feng, W.; Tsang, I.; and Wang, S. 2023. Leveraging inpainting for single-image shadow removal. In *Proceedings of the IEEE/CVF International Conference on Computer Vision*, 13055–13064.
- Li, Z.; Xie, G.; Jiang, G.; and Lu, Z. 2025. Shadowmask-former: Mask augmented patch embedding for shadow removal. *IEEE Transactions on Artificial Intelligence*.
- Liu, Y.; Ke, Z.; Xu, K.; Liu, F.; Wang, Z.; and Lau, R. W. 2024a. Recasting regional lighting for shadow removal. In *Proceedings of the AAAI Conference on Artificial Intelligence*, volume 38, 3810–3818.
- Liu, Y.; Tian, Y.; Zhao, Y.; Yu, H.; Xie, L.; Wang, Y.; Ye, Q.; Jiao, J.; and Liu, Y. 2024b. Vmamba: Visual state space model. *Advances in neural information processing systems*, 37: 103031–103063.
- Lu, S.; Ding, Y.; Liu, M.; Yin, Z.; Yin, L.; and Zheng, W. 2023. Multiscale feature extraction and fusion of image and text in VQA. *International Journal of Computational Intelligence Systems*, 16(1): 54.
- Lu, Y.; Wang, S.; Wang, Z.; Xia, P.; Zhou, T.; et al. 2024. LF-Mamba: light field image super-resolution with state space model. *arXiv preprint arXiv:2406.12463*.
- Mirza, M.; and Osindero, S. 2014. Conditional generative adversarial nets. *arXiv preprint arXiv:1411.1784*.
- Nadimi, S.; and Bhanu, B. 2004. Physical models for moving shadow and object detection in video. *IEEE transactions*



on pattern analysis and machine intelligence, 26(8): 1079–1087.

Nasiri-Sarvi, A.; Trinh, V. Q.-H.; Rivaz, H.; and Hosseini, M. S. 2024. Vim4path: Self-supervised vision mamba for histopathology images. In *Proceedings of the IEEE/CVF Conference on Computer Vision and Pattern Recognition*, 6894–6903.

Özdemir, Ö.; and Akagündüz, E. 2024. Enhancing visual question answering through question-driven image captions as prompts. In *Proceedings of the IEEE/CVF Conference on Computer Vision and Pattern Recognition*, 1562–1571.

Pang, T.; Zheng, H.; Quan, Y.; and Ji, H. 2021. Recorruped-to-recorruped: Unsupervised deep learning for image denoising. In *Proceedings of the IEEE/CVF conference on computer vision and pattern recognition*, 2043–2052.

Qiao, J.; Liao, J.; Li, W.; Zhang, Y.; Guo, Y.; Wen, Y.; Qiu, Z.; Xie, J.; Hu, J.; and Lin, S. 2024. Hi-mamba: Hierarchical mamba for efficient image super-resolution. *arXiv preprint arXiv:2410.10140*.

Qu, L.; Tian, J.; He, S.; Tang, Y.; and Lau, R. W. 2017. Deshadownet: A multi-context embedding deep network for shadow removal. In *Proceedings of the IEEE conference on computer vision and pattern recognition*, 4067–4075.

Ren, Y.; Li, X.; Guo, M.; Li, B.; Zhao, S.; and Chen, Z. 2024. MambaCSR: Dual-Interleaved Scanning for Compressed Image Super-Resolution With SSMs. *arXiv preprint arXiv:2408.11758*.

Sarem, M.; Jurdi, T.; Albshlawy, L.; and Massrie, E. 2024. Improving long text classification based on Selective State Space model (Mamba). In *2024 IEEE 17th International Symposium on Embedded Multicore/Many-core Systems-on-Chip (MCSoc)*, 32–38. IEEE.

Vasluianu, F.-A.; Seizinger, T.; Zhou, Z.; Wu, Z.; Chen, C.; Timofte, R.; Dong, W.; Zhou, H.; Tian, Y.; Chen, J.; et al. 2024. NTIRE 2024 image shadow removal challenge report. In *Proceedings of the IEEE/CVF Conference on Computer Vision and Pattern Recognition*, 6547–6570.

Vaswani, A.; Shazeer, N.; Parmar, N.; Uszkoreit, J.; Jones, L.; Gomez, A. N.; Kaiser, Ł.; and Polosukhin, I. 2017. Attention is all you need. *Advances in neural information processing systems*, 30.

Wan, J.; Yin, H.; Wu, Z.; Wu, X.; Liu, Y.; and Wang, S. 2022. Style-guided shadow removal. In *European Conference on Computer Vision*, 361–378. Springer.

Wang, J.; Li, X.; and Yang, J. 2018. Stacked conditional generative adversarial networks for jointly learning shadow detection and shadow removal. In *Proceedings of the IEEE conference on computer vision and pattern recognition*, 1788–1797.

Xiao, J.; Fu, X.; Zhu, Y.; Li, D.; Huang, J.; Zhu, K.; and Zha, Z.-J. 2024a. Homoformer: Homogenized transformer for image shadow removal. In *Proceedings of the IEEE/CVF Conference on Computer Vision and Pattern Recognition*, 25617–25626.

Xiao, Y.; Yuan, Q.; Jiang, K.; Chen, Y.; Zhang, Q.; and Lin, C.-W. 2024b. Frequency-assisted mamba for remote sensing image super-resolution. *IEEE Transactions on Multimedia*.

Xu, J.; Li, Z.; Zheng, Y.; Huang, C.; Gu, R.; Xu, W.; and Xu, G. 2025. Omnisr: Shadow removal under direct and indirect lighting. In *Proceedings of the AAAI Conference on Artificial Intelligence*, volume 39, 8887–8895.

Yang, J.; Lu, J.; Lee, S.; Batra, D.; and Parikh, D. 2018. Graph r-cnn for scene graph generation. In *Proceedings of the European conference on computer vision (ECCV)*, 670–685.

Zhang, X.; Ma, J.; Shahin, M.; Ahmed, B.; and Epps, J. 2025. Rethinking mamba in speech processing by self-supervised models. In *ICASSP 2025-2025 IEEE International Conference on Acoustics, Speech and Signal Processing (ICASSP)*, 1–5. IEEE.

Zhu, X.; Chow, C.-O.; and Chuah, J. H. 2024. ShadowMamba: State-Space Model with Boundary-Region Selective Scan for Shadow Removal. *arXiv preprint arXiv:2411.03260v1*.

Zhu, Y.; Huang, J.; Fu, X.; Zhao, F.; Sun, Q.; and Zha, Z.-J. 2022. Bijective mapping network for shadow removal. In *Proceedings of the IEEE/CVF Conference on Computer Vision and Pattern Recognition*, 5627–5636.

Zhu, Z.; Chen, Y.; Zhang, S.; Luo, G.; and Zeng, J. 2025. Mamba-based Unet for Hyperspectral Image Denoising. *IEEE Signal Processing Letters*.

Zou, W.; Jiang, M.; Zhang, Y.; Chen, L.; Lu, Z.; and Wu, Y. 2021. Sdwnet: A straight dilated network with wavelet transformation for image deblurring. In *Proceedings of the IEEE/CVF international conference on computer vision*, 1895–1904.

## A. Evaluation Metrics

To enable quantitative comparisons with existing methods, we follow previous studies (Zhu et al. 2022; Fu et al. 2021; Le and Samaras 2021; Wan et al. 2022) and adopt RMSE in the LAB color space to evaluate shadow removal performance. This metric measures the difference between the predicted shadow-free images and the ground truth, where a lower RMSE indicates better restoration quality. In addition, to assess performance in the RGB color space, we also employ PSNR and SSIM as evaluation metrics. All images used for evaluation are uniformly resized to 256×256 to ensure consistency across comparisons.

## B. Quantitative Results on the ISTD dataset

In this section, we present the detailed quantitative results of shadow removal on the ISTD dataset, comparing our method, D2-Mamba, with several recent state-of-the-art techniques. We compute PSNR, SSIM, and RMSE for the shadow region (S), non-shadow region (NS), and the entire image (ALL).

As shown in Table 4, D2-Mamba demonstrates competitive performance across all these categories. Specifically, in the shadow region (S), our method achieves a PSNR of 39.14, SSIM of 0.992, and RMSE of 5.61, outperforming most state-of-the-art techniques, indicating its ability to effectively remove shadows while preserving image details. In the non-shadow region (NS), D2-Mamba achieves the

Method	Shadow Region (S)			Non-Shadow Region (NS)			All Image (ALL)		
	PSNR $\uparrow$	SSIM $\uparrow$	RMSE $\downarrow$	PSNR $\uparrow$	SSIM $\uparrow$	RMSE $\downarrow$	PSNR $\uparrow$	SSIM $\uparrow$	RMSE $\downarrow$
DHAN (Chen et al. 2021)	34.65	0.983	8.26	29.81	0.937	5.56	28.15	0.913	6.37
BMNet (Zhu et al. 2022)	35.61	0.988	7.60	32.80	0.976	4.59	30.28	0.959	5.02
ShadowFormer-S (Guo et al. 2023a)	37.99	0.990	6.16	<u>33.89</u>	0.980	<u>3.90</u>	31.81	0.967	4.27
ShadowDiffusion (Guo et al. 2023b)	<b>40.15</b>	<b>0.994</b>	<b>4.13</b>	33.70	0.977	4.14	<b>32.33</b>	<b>0.969</b>	<u>4.12</u>
HomoFormer (Xiao et al. 2024a)	39.07	0.991	5.64	33.45	<u>0.979</u>	4.10	31.82	<u>0.968</u>	4.33
ShadowMamba (Zhu, Chow, and Chuah 2024)	38.01	0.990	5.95	33.78	0.974	3.90	31.79	0.960	4.23
ShadowMaskFormer (Li et al. 2025)	-	-	6.08	-	-	3.86	-	-	4.23
ShadowGAN-Former (Hu et al. 2025)	36.64	0.990	6.82	33.60	0.980	4.00	30.97	0.967	4.46
MSRDNet (Huang et al. 2025)	37.36	0.989	6.38	33.38	0.980	4.09	31.16	0.965	4.48
OmniSR (Xu et al. 2025)	-	-	-	-	-	-	31.56	0.965	-
D2-Mamba (Ours)	<u>39.14</u>	<u>0.992</u>	<u>5.61</u>	<b>34.10</b>	<b>0.981</b>	<b>3.81</b>	<u>32.18</u>	<b>0.969</b>	<b>4.06</b>

Table 4: The quantitative results of shadow removal using our models and recent methods on the ISTD dataset.

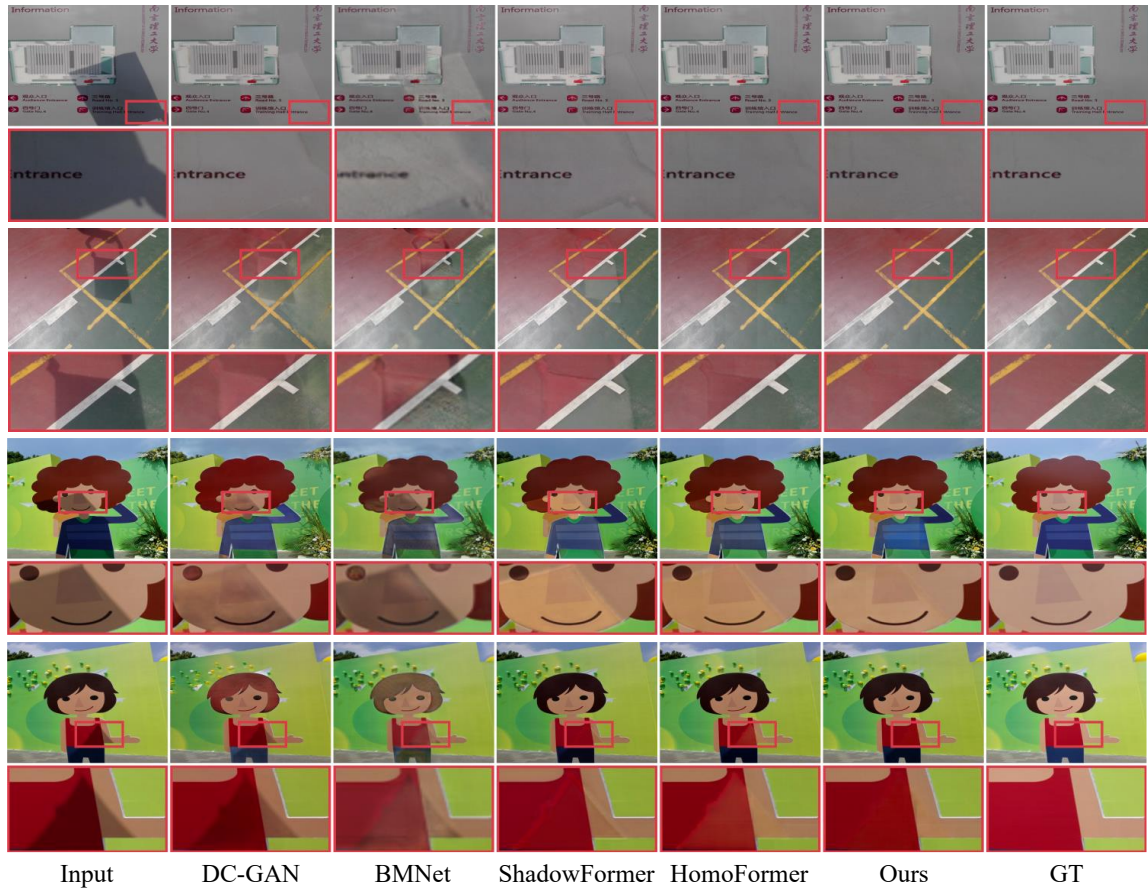


Figure 5: Visual examples of the shadow removal results on the ISTD.

Method	Shadow Region (S)			Non-Shadow Region (NS)			All Image (ALL)		
	PSNR $\uparrow$	SSIM $\uparrow$	RMSE $\downarrow$	PSNR $\uparrow$	SSIM $\uparrow$	RMSE $\downarrow$	PSNR $\uparrow$	SSIM $\uparrow$	RMSE $\downarrow$
MAS $\rightarrow$ HS	38.98	0.991	5.75	33.86	0.980	3.92	32.04	0.968	4.20
HS $\rightarrow$ MAS	39.15	0.992	5.51	33.98	0.980	3.80	32.16	0.969	4.06

Table 5: Ablation study of the path execution order on the ISTD.

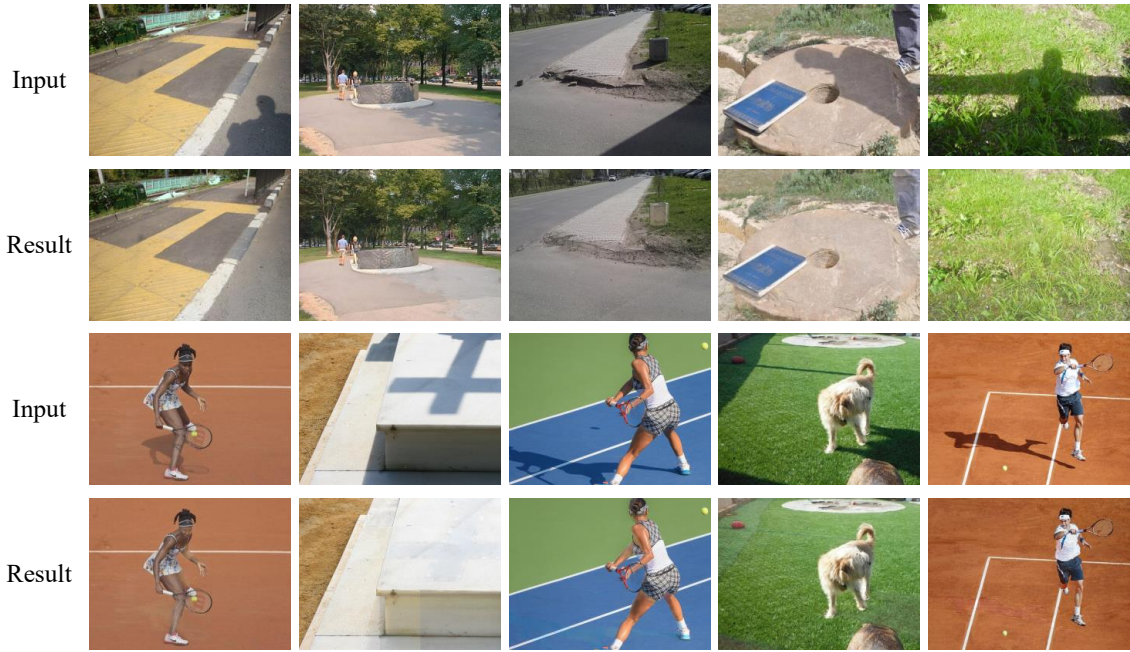


Figure 6: Shadow removal results of the proposed D2-Mamba on the SBU Shadow Dataset. Each pair shows the input shadow image and the corresponding shadow-free result produced by our model. The results demonstrate the model’s ability to handle complex shadow patterns under diverse real-world indoor lighting conditions.

best results with a PSNR of 34.10, SSIM of 0.981, and a low RMSE of 3.81, highlighting its strength in preserving the quality of the non-shadowed areas. Additionally, in terms of overall image quality (ALL), D2-Mamba maintains a PSNR of 32.18, SSIM of 0.969, and RMSE of 4.06, consistently outperforming many competing methods. These results demonstrate that D2-Mamba offers significant advantages over existing methods, providing excellent shadow removal performance while preserving image quality in both shadow and non-shadow regions. This makes D2-Mamba a strong candidate for real-world shadow removal tasks.

### C. Qualitative Results on the ISTD dataset

To further validate the effectiveness of the proposed D2-Mamba framework, we present qualitative results on the ISTD dataset in Figure 5. As shown in the visual comparisons, our method produces cleaner shadow-free images with fewer residual artifacts compared to existing approaches. D2-Mamba demonstrates strong performance in preserving texture details and structural consistency across both shadow and non-shadow regions. The removed shadow areas appear visually natural and seamlessly integrated with the surrounding context.

For example, in the first two examples, the first four methods exhibit noticeable artifacts, where the shadow-removed regions fail to blend naturally with the background. In the third image, due to the presence of complex shadow patterns, the compared methods produce results with significant color inconsistencies within the shadowed areas. In the last two images, these methods struggle to restore the true color of the shadow regions, resulting in residual shadows or visi-

ble color distortions.

These qualitative results demonstrate that D2-Mamba achieves a more accurate and visually coherent shadow removal, highlighting its strong capacity to model both global semantic structure and local shadow variations.

### D. Ablation Study on the Path Execution Order in our proposed DPMG module

As shown in Table 5, we investigated the execution order of the two pathways in the DPMG module and reached a key conclusion: the model achieves better performance when the horizontal scanning path precedes the mask-aware adaptive scanning path, compared to the reverse order.

This finding suggests that the horizontal scanning path plays a crucial role as the initial step for global information extraction. A potential explanation is that the horizontal scanning path allows the model to first capture comprehensive contextual information, which provides a solid foundation for the subsequent fine-grained shadow removal. By understanding the overall structure of the image, the model can more effectively distinguish shadowed from non-shadowed regions, leading to more accurate shadow detail recovery during the mask-aware adaptive scanning stage.

In contrast, when the mask-aware adaptive scanning path is executed first, the model may overly focus on local shadow information while missing essential global context. This can result in inconsistencies or distortions when processing complex shadow patterns, ultimately degrading both the precision of shadow removal and structural continuity.

In summary, placing the horizontal scanning path first

Model	Param(M)	FLOPs(G)	Infer(ms)	Mem(GB)
ShadowMaskFormer (Li et al. 2025)	2.28	47.79	42	9.29
ShadowDiffusion (Guo et al. 2023b)	55	364.12	70	12.99
HomoFormer (Xiao et al. 2024a)	17.18	71.25	23	7.40
ShadowFormer-L(Guo et al. 2023a)	11.35	129.20	38	6.93
Ours	9.39	40.09	42	11.69

Table 6: Complexity comparison with recent models.

provides the model with a better global understanding, which in turn allows the subsequent mask-aware adaptive scanning to perform more accurate and structurally coherent shadow removal tasks.

### E. Extensive Results on the SBU Dataset

To further evaluate the adaptability of the proposed D2-Mamba model in complex scenarios, we conducted additional qualitative experiments on the SBU Dataset. This dataset presents more challenging conditions, containing diverse indoor lighting environments with complex shadow distributions cast by objects such as people and furniture. Figure 6 illustrates several shadow removal examples produced by our model on selected images from the SBU dataset. These results demonstrate that D2-Mamba not only performs well on standard benchmark datasets but also exhibits strong generalization ability and robustness, making it suitable for shadow removal tasks in more diverse and dynamic real-world environments.

### F. Complexity Comparison

Table 6 shows the parameter count, computational complexity, inference time, and memory usage. The parameter count (Param(M)) and computational complexity (FLOPs(G)) are calculated using the thop library. Our model ("Ours") has a relatively low parameter count and good FLOPs, striking a balance between computational complexity and performance, with a short inference time.